Structure of Monodisperse and Bimodal Brushes

E. P. K. Currie,*,† M. Wagemaker,‡ M. A. Cohen Stuart,† and A. A. van Well‡

Department of Physical and Colloid Chemistry, Wageningen University, The Netherlands, and Interfaculty Reactor Institute, Delft University of Technology, The Netherlands

Received June 11, 1999; Revised Manuscript Received September 27, 1999

ABSTRACT: The structure of monodisperse and bimodal brushes consisting of poly(ethylene oxide) (PEO) at the air/water interface is investigated with neutron reflectivity, and the results are compared with the structure predicted by the Scheutjens−Fleer self-consistent-field lattice model. The monomer density profile of a monodisperse PEO brush at low and intermediate grafting densities is block-like with an extended tail region in which the density smoothly decays to zero. At high grafting densities, however, the profile is predominantly parabolic, as predicted by analytical self-consistent-field models. Quantitative agreement is found between the experimentally measured profiles and those predicted by the Scheutjens−Fleer model. Bimodal brushes are investigated for three chain length ratios and mixing ratios at various grafting densities. It is concluded that at a given grafting density, the long chains are more extended in bimodal brushes than in monodisperse brushes at the same grafting density. This additional stretching increases with increasing length of the smaller block or increasing fraction of smaller blocks. The agreement between the Scheutjens−Fleer and measured density profiles is also good in the case of bimodal brushes.

1. Introduction

Linear polymers end-grafted to an interface at high grafting densities (so-called brushes) in contact with a good solvent have been investigated in numerous studies in the past decade. A key issue is the monomer density profile (i.e., the variation in the monomer density as a function of the distance from the grafting plane). Initially, scaling models assumed the monomer density to be constant throughout the brush (the so-called box model).[1,2] Using an analytical self-consistent-field (aSCF) model Milner et al.[3] and Zhulina et al.[4] demonstrated that the monomer density decreases parabolically from a finite value at the grafting plane to zero at the edge of the brush. The predicted scaling laws in the aSCF model for the brush height H and surface pressure π as a function of the chain length N and grafting density σ are $H \sim N\sigma^{1/3}$ and $\pi \sim N\sigma^{5/3}$ (where σ is defined as the number of chains per unit area).

The aSCF model, however, only considers the most probable polymer conformation of quasi-infinitely long chains. Fluctuations of chain ends at the brush edge and interactions of monomers with the grafting plane are not taken into account. Numerical SCF (nSCF) and molecular dynamics studies demonstrated that in the case of nonadsorbing polymers, a depletion zone appears close to the grafting plane because the impermeability of the grafting plane is entropically unfavorable.[5−9] At the edge of the brush an extended tail region is found, which is the averaged result of large fluctuations in the conformation of the chain ends. These fluctuations originate from the fact that the chain ends are weakly stretched in this distal region.[8,9] The monomer density in the tail region drops exponentially to zero with increasing distance from the grafting plane. In nSCF calculations, the importance of such fluctuations decreases with increasing chain length and increasing grafting density, as the degree of stretching of the chains increases with increasing grafting density. The nSCF density profile of long chains at high grafting densities thus closely resembles the parabolic profile predicted by the aSCF model.[7]

Polymer brushes can be investigated experimentally with small angle neutron scattering (SANS) and neutron reflectivity (NR).[10−18] The information obtained from NR is the spatial distribution of components perpendicular to the reflecting interface, which is defined here as the z-direction. The characteristic length scale for which information may be obtained is ∼1−1000 nm. The reflectivity is measured as a function of the wavevector component perpendicular to the interface $q = 2\pi \sin \theta/\lambda$, where λ is the neutron wavelength and θ is the angle of reflection. The measured reflectivity $R(q)$ depends on the neutron refractive index profile perpendicular to the interface.[19] Because the neutron refractive index is directly related to the scattering length density nb (where n is the particle number density and b the sum of the scattering lengths of the specific nuclei in the particle), NR probes the number density profile $n(z)$ with high spatial resolution. Subsequently, $n(z)$ can be related to the volume fraction profile of the components in the interfacial layer. In the case of polymer brushes, this corresponds with the monomer density distribution throughout the brush.

The overall brush properties in various systems (the brush height H as a function of N and σ) have been examined with SANS and NR.[10,11,13−16,18] The density profile of the brush was not considered in detail in these references. The results of Auroy et al. for H as a function of N and σ agreed with the aSCF scaling laws, whereas others reported no agreement with the same scaling laws.[13,17,18]

Karim et al.[15] found a parabolic profile, corrected with a tail region, for long polystyrene (PS) brushes in toluene. In this study, however, a single grafting density was considered for various solvent qualities, and the scaling laws for H and π were not examined. Field et al.[12] also considered the density profiles, but had four different chain lengths at a fixed grafting density. Both studies showed a parabolic profile to fit the data well,

* To whom correspondence should be addressed. E-mail: CURRIE@FENK.WAU.NL. Telephone: 00-31-317-482178.
† Department of Physical and Colloid Chemistry.
‡ Interfaculty Reactor Institute.

10.1021/ma990936w CCC: $18.00
Published on Web 12/04/1999

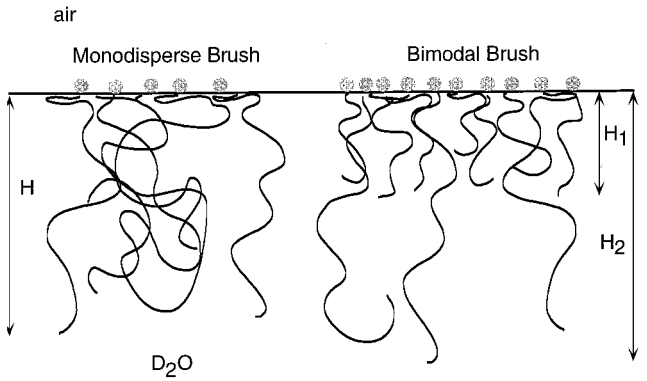

Figure 1. A graphic representation of a monodisperse and a bimodal PEO brush at the air/water interface. The gray spheres represent the PS anchoring blocks, and H_1 and H_2 represent the thickness of the layer of relatively short and long chains, respectively.

although Field et al.[12] also reported a good fit with an error function.

Bijsterbosch et al.[18] used various polystyrene−poly(ethylene oxide) (PS−PEO) diblock copolymers deposited on an air/water interface to prepare model brush systems. The aSCF scaling laws for the brush height as a function of σ did not agree; a scaling exponent of 0.41 instead of 0.33 was reported. In a recent paper, however, we showed that the PEO brushes do corroborate the predicted aSCF scaling laws for the brush height and surface pressure, provided (*i*) long chains are used ($N \gtrsim 450$), (*ii*) the grafting density is high enough and known accurately, and (*iii*) the surface activity of the grafted chain (in this case the PEO block) is taken into account.[20] When these conditions are not met, validation of the brush scaling laws is likely to give erroneous results. Using the Scheutjens−Fleer nSCF model, the surface pressure isotherms of the PS−PEO brushes were modeled.[20] These numerical isotherms showed good agreement with the experimental isotherms.

In this paper, we examine the structure of the PEO brushes with NR under conditions where the aSCF scaling laws are expected to be valid, using our previous results.[20] The brush of a known chain length is investigated at various grafting densities. The grafting density is varied at fixed chain length via compression of the polymeric layer in a Langmuir trough. To interpret all data in a consistent way, the density profiles obtained from NR fits are compared with the nSCF profiles using the same parameter set that gives good agreement between experimental and numerical surface pressure isotherms.

The brush architecture can be varied by mixing two different chain lengths at a certain mixing ratio, resulting in a so-called bimodal brush. Such brushes can be considered model systems for polydisperse brushes that contain several different chain lengths. Analyses of bimodal brushes of chain lengths N_l and N_s with aSCF and nSCF models demonstrate that, provided the ratio N_l/N_s is large and the mixing ratio within 'reasonable' limits, the brush effectively consists of two regions: (*i*) a proximal region close to the grafting plane in which the shorter chains reside and in which the longer chains are locally highly stretched, and (*ii*) a distal region in which the bulk of the monomers of the longer chains is found.[21−24] A schematic illustration of a monodisperse and a bimodal brush is given in Figure 1. Variation of the grafting density, mixing ratios, and length ratios of the chains affects the structure of the grafted layer.

In this paper, the density profiles of bimodal PEO brushes at the air/water interface are also analyzed by NR and compared with nSCF calculations. Comparison of the nSCF density profiles with those obtained by analysis of the NR spectra may provide insight in the brush architecture.

The structure of the paper is as follows: in *Section 2*, the experimental details of the preparation of PEO brushes, the analysis of the NR data and the nSCF model are briefly discussed. In *Section 3*, the results for monodisperse brushes are examined, and in *Section 4* those of bimodal brushes are reviewed. Finally, in *Section 5*, we discuss the results and present our conclusions.

2. Materials and Methods

The PS−PEO block copolymers were synthesized in the group of Dr. G. Riess, Mulhouse, France.[25] The polymers used in this study consist of a PS group of 38 monomers and of a PEO group of 148, 250, and 700 monomers. The reported polydispersities are 1.15, 1.2, and 1.25, respectively. The block copolymers were dissolved in chloroform and deposited on an air/D_2O interface in a Langmuir trough using a Hamilton microsyringe. The D_2O (99.8 %) was purchased from Acros. The surface pressure of the interface was measured with a Wilhelmy plate during the NR measurements. All measurements of the spread layers were performed at room temperature. Because a small fraction of the polymer sample consists of PEO homopolymer, the polymer layer was first compressed far above the saturated surface pressure of PEO (i.e., 10 mN m^{-1}).[20,28] This procedure ensures that the homopolymer is forced into the water phase and the remaining monolayer consists solely of PS−PEO block copolymer. The surface pressure of the resultant layer remained constant during measurement, indicating that the polymeric layer is stable and that no material, other than the PEO homopolymer, is lost during measurement. More details on the preparation of PS−PEO monolayers are given in ref 18.

The NR measurements were performed on SURF at ISIS, Rutherford Appleton Laboratory, U.K. Three reflection angles were used, 0.4°, 0.8° and 1.5°, and the periods of measurement were 30, 100, and 200 min, respectively. The information obtained with NR is the spatial distribution of components perpendicular to the reflecting interface. In only detecting the specular reflected beam, the information in plane with the reflecting interface is lost. The reflectivity is measured as a function of the wave vector component perpendicular to the interface $q = (2\pi/\lambda) \sin \theta$, where λ is the neutron wavelength and θ is the angle of reflection. The reflectivity $R(q)$ depends on the neutron refractive index profile perpendicular to the interface, which is defined here as the *z*-direction. The neutron refractive index is directly related to the scattering length density (SLD), $\Gamma = 4\pi nb$, where n is the particle number density and b the sum of the scattering lengths of the specific nuclei in the particle.

Because the phase information is lost in the neutron detection, inversion from a certain reflectivity spectrum $R(q)$ to a SLD profile is not direct, and is usually done by fitting a chosen model to the experimental data. The model of the SLD depth profile is divided in a chosen

number of layers, and for each layer the thickness, SLD and interfacial roughness can be fitted. Under the assumption of ideal mixing (no volume contraction on dissolvement); the SLD profile of a polymer adsorbed or end-grafted at the air solvent interface can be expressed in terms of the volume fraction $\rho(z)$ of the polymer, the SLD Γ_p of pure polymer and that of pure solvent Γ_s, according to

$$\Gamma(z) = \rho(z)\Gamma_p + (1 - \rho(z))\Gamma_s \quad (1)$$

In summary, the measured neutron reflectivity of the grafted polymeric layer can be related to a depth profile of the polymer volume fraction.

In this paper the NR spectra were interpreted by weighted least-squares fitting of the calculated model reflectivity to the experimental data. The NR spectra of the monodisperse brush in D_2O were analyzed with two models for the volume fraction of the tail region; namely, a parabolic profile,

$$\rho(z) = \rho(0)\left(1 - \frac{z^2}{H^2}\right) \quad (2)$$

for $z \leq H$, and a block profile (single layer) with roughness

$$\rho(z) = \rho_b\left(1 - \mathrm{erf}((z - H)/\varsigma_b\sqrt{2})\right) \quad (3)$$

where ρ_b is the volume fraction of the polymer block, and H is the brush thickness. The tail region of the adsorbed polymers is modeled by an error function,[26] where ς_b is a measure for the decay length of the roughness. During fitting, the error function is cut off within the thickness of the smallest layer. Therefore, ς_b should be smaller than the layer thickness not to give large discontinuities in $\rho(z)$. In the case of bimodal brushes, $\rho(z)$ is simply the sum of either two parabolic profiles, two block profiles, or a combination of both, with each parabola characterized by $\rho(0)$ and H, and each block characterized by ρ_b, H, and ς_b.

The interface of the solution with the air was also modeled with an error function, resulting in the following model for the SLD:

$$\Gamma(z) = \left(\rho(z)\Gamma_p + (1 - \rho(z))\Gamma_s\right)\mathrm{erf}(z/\varsigma_{int}\sqrt{2}) \quad (4)$$

In the PS−PEO monolayer, the roughness of the interface consists of three contributions: (*i*) the generic roughness of an air/water interface, (*ii*) the monolayer of adsorbed PEO at the interface,[20] and (*iii*) the collapsed PS blocks. Characterization of these three contributions with a single ς_{int} would appear to be incomplete as there seems to be no direct relationship between the PS blocks, the adsorbed PEO layer, and σ. There are two arguments, however, that allow us to model the contributions just mentioned to the total SLD with a single roughness parameter. First, neutrons with a wave vector component perpendicular to the interface q probe length scales in the z-direction in the order of π/q. Because the contribution of the neutrons in a high q-range to the reflectivity is relatively small, the q-range in which relevant information is obtained is limited by the background signal. In our case, this background signal was the dominant contribution for values >1.2 nm^{-1}. Thus, the information on the structure of the interface obtained from the reflectivity profile is limited. The second argument is that Γ_{PEO} and Γ_{PS} are small compared with Γ_{D_2O} (Γ_{PEO} is 0.75 10^{-3} nm^{-2}, that of PS is 1.76 10^{-3} nm^{-2}, whereas that of D_2O is 7.96 10^{-3} nm^{-2}). It is therefore mainly solvent depletion (the second term in eq (4)) that determines the total SLD near the interface. The conclusion of both arguments is that the overall contribution of the PS and PEO at the air/water interface to the reflectivity profile is small compared with the SLD of the thick brush layer, so that the interfacial roughness can be approximated by a single roughness parameter.

In the experiments presented in this paper, the brush region is the subject of interest, rather than the thin adsorbed surface layer. If instead one would be interested the structure of this thin layer, then it can be highlighted by selectively substituting deuterium atoms for hydrogen atoms in the polymer groups of interest in combination with solvent contrast variation. This is already a well-established technique in revealing thin layer structures.[27]

The nSCF calculations were done with the Scheutjens−Fleer SCF lattice model. Details of this model are given in ref 20. In short, the monomer density at a given distance z from the grafting plane must be self-consistent with the Boltzmann-like potential field it generates. Thus, a density profile $\rho(z)$ is found for a given grafting density, chain length, solvent quality, and adsorption strength to the grafting plane. In the numerical calculations, the solvent quality is taken to be good, which is the case for PEO in water.[29,30] As mentioned, PEO is surface active (i.e., it adsorbs at the air/water interface). Therefore, an adsorption strength of 1 k_BT per monomer is assigned to the grafted chain[20] where k_B is the Boltzmann constant and T the temperature. This value is close to the estimated experimental value of PEO at the air/water interface,[18] but was not adjusted for a best fit to the surface pressure data (a slightly higher adsorption energy gives a better fit). The number of monomers in the calculations is equal to those used experimentally, and the length of the cubic lattice cell is equal to the length of a PEO monomer (0.35 nm).[29] We again stress that no fit parameters were used in the nSCF calculations; that is, all values were those reported experimentally in the literature.

3. Monodisperse Brushes

We start by comparing the experimental surface pressure isotherms of the PS−PEO layer with the nSCF isotherms for two of the PEO chain lengths used (250 and 700 monomers).[20] The experimental surface pressure isotherms are the solid lines and the nSCF isotherms are the dashed lines in Figure 2. The good agreement between the experimental and numerical isotherms indicates that thermodynamic parameters of the polymeric monolayer, such as the surface pressure, are adequately modeled in the nSCF model. Stars in Figure 2 indicate the surface pressure at which the NR measurements were done for monodisperse brushes of 700 monomers. Previous analysis showed that the onset of the brush regime of PEO brushes at the air/water interface is found at $\pi \approx 10$ mN m^{-1}.[20] It is clear that the surface pressure at the densities at which the NR measurements were performed is well above this value.

The measured reflectivities R of the PS−PEO layer are plotted semilogarithmically in Figure 3a for two grafting densities as a function of q, together with the reflectivity of pure D_2O. The curve drawn through the

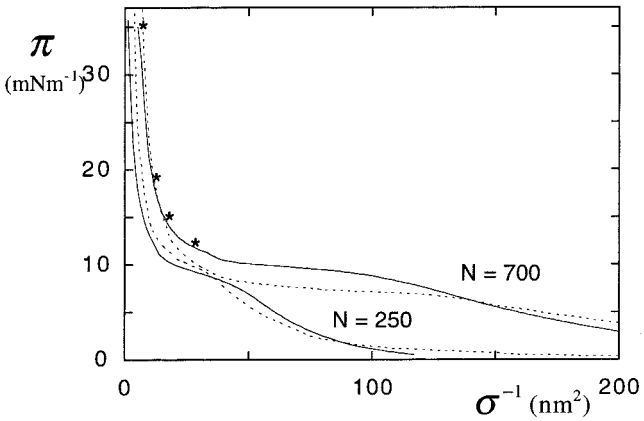

Figure 2. The experimental (solid curve) and nSCF (dashed curve) surface pressure isotherm for monodisperse PEO brushes. The stars indicate the grafting densities at which NR reflectivities were measured.

symbols is a guide to the eye. The inset in Figure 3a shows a part of $R(q)$ in more detail. It is clear that the reflectivity curves of the PEO brushes are significantly more irregular than the smooth Fresnel curve of D_2O, and that this irregularity is enhanced with increasing grafting density.

This enhanced irregularity is shown more clearly in Figure 3b, where the ratio of the reflectivities $R(q)$ and that of the D_2O bulk phase $R_{D_2O}(q)$ is plotted for three grafting densities. Evidently, as σ increases the ratio R/R_{D_2O} is expected to decrease, as $\Gamma_{PEO} < \Gamma_{D_2O}$. This decrease is observed in Figure 3b, where R/R_{D_2O} decreases strongly as the area per molecule decreases.

In Figure 3c $R(q)q^4$ is plotted as a function of q. We remark that for clarity, $2\ 10^{-6}$ has been added to the value of $R(q)q^4$ in the spectrum corresponding to 18 nm^2 per molecule, and 10^{-6} to that corresponding to 11.8 nm^2 per molecule in Figure 3c.

Representation of the grafted PEO layer as a single block with an uniform scattering length density (i.e., a grafted layer of constant monomer density with no roughness) gave no reasonable fit of the NR spectra for any value of σ. This result implies that the decrease in monomer density in the brush is gradual and not abrupt, which is in agreement with earlier results.[12,15] In Table 1 the values of the fit parameters that give the best fit for a parabolic profile and for a block with roughness are listed. The corresponding areas per molecule are given, together with the surface pressure of the polymeric monolayer (in mN m^{-1}). The ς_{int} is the roughness of the interface (nm), H is the height of either the parabolic profile or the block (nm), ρ is either the (dimensionless) monomer density at the interface ($\rho(0)$ in the case of a parabolic profile, or the block density ρ_b in the case of a block profile), Γ_{D_2O} is the scattering length density of the subphase, and χ^2 is the fit quality, renormalized with respect to the χ^2 of the pure D_2O fit. The overall best fit (parabolic or rough block) for a given grafting density, corresponding to the lowest value of χ^2, is shown in bold face in Table 1.

As stated in *Section 2*, the roughness of the interface of the PS−PEO monolayer consists of three contributions: (*i*) the generic roughness of an air/water interface, (*ii*) the monolayer of adsorbed PEO at the interface,[20] and (*iii*) the collapsed PS blocks. In the brush regime, the first two contributions to the interface roughness remain approximately constant as σ increases, whereas the third contribution evidently increases with increasing σ. As these three contributions are modeled with ς_{int}, ς_{int} is expected to increase with increasing σ. This expectation is confirmed in Table 1, where ς_{int} is shown to increase with decreasing area per PEO chain.

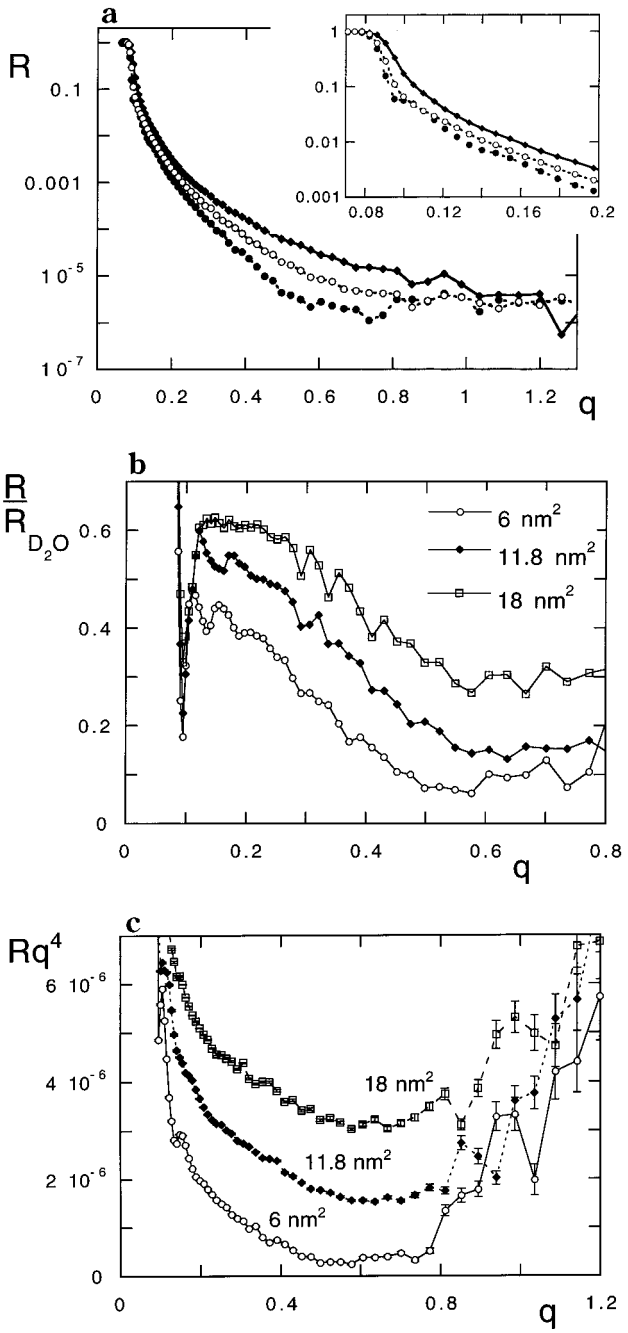

Figure 3. The reflectivity spectra of the PEO brushes ($N = 700$): (a) plotted semilogarithmically as a function of q (in nm^{-1}) for 18 nm^2 per PS−PEO molecule (open circles) and 6 nm^2 (closed circles), together with that of D_2O (diamonds); (b) plotted with respect to that of D_2O for three densities; and (c) plotted as Rq^4, with error bars. For clarity, the data in Figure 3c corresponding to 11.8 nm^2 and 18 nm^2 per molecule have been shifted by 10^{-6} and 210^{-6}, respectively.

It is instructive to compare the reflectivity curves of the fits of the parabolic and block profiles with the experimental measured reflectivities. In Figure 4a these curves for the best parabolic fits are plotted as $R(q)q^4$ versus q in the low q range for three grafting densities; namely, 6, 11.8, and 18 nm^2 per molecule. (In the following, low and high σ denote the lowest and highest measured grafting density, respectively. Low σ does not

Table 1. Neutron Reflectivity Results for Monodisperse PEO Brushes[a]

area	π	fit	ς_{int}	H	ρ	ς_b	$\Gamma_{D_2O}\cdot10^3$	χ^2
D20	0		0.27(2)				7.96(2)	1
18 nm^2	13.8	**block**	1.01(2)	26.3(8)	0.0818(3)	8(1)	7.35(2)	0.41
		parabola	0.97(2)	34(1)	0.0818(4)		7.33(2)	1.10
14.5 nm^2	15.8	**block**	1.16(3)	33(1)	0.12(1)	11(1)	7.44(2)	0.54
		parabola	1.12(2)	41(1)	0.0938(4)		7.38(2)	0.67
11.8 nm^2	18.5	**block**	1.20(2)	33.3(6)	0.121(3)	10.1(7)	7.35(2)	0.54
		parabola	1.20(2)	44.4(9)	0.106(4)		7.19(2)	0.80
6.0 nm^2	35.2	block	1.61(2)	40(1)	0.167(3)	10.1(9)	7.26(2)	1.72
		parabola	1.59(2)	52.2(6)	0.133(5)		7.07(2)	0.94

[a] $N = 700$, with the surface pressure π (mN m^{-1}), surface roughness ς_{int} (nm), brush height H (nm), monomer density ρ, roughness block ς_b (nm), scattering length density solvent (nm^{-2}), and fit quality χ^2 with respect to the fit of pure D_2O (the notation 0.27(2) denotes 0.27 ± 0.02).

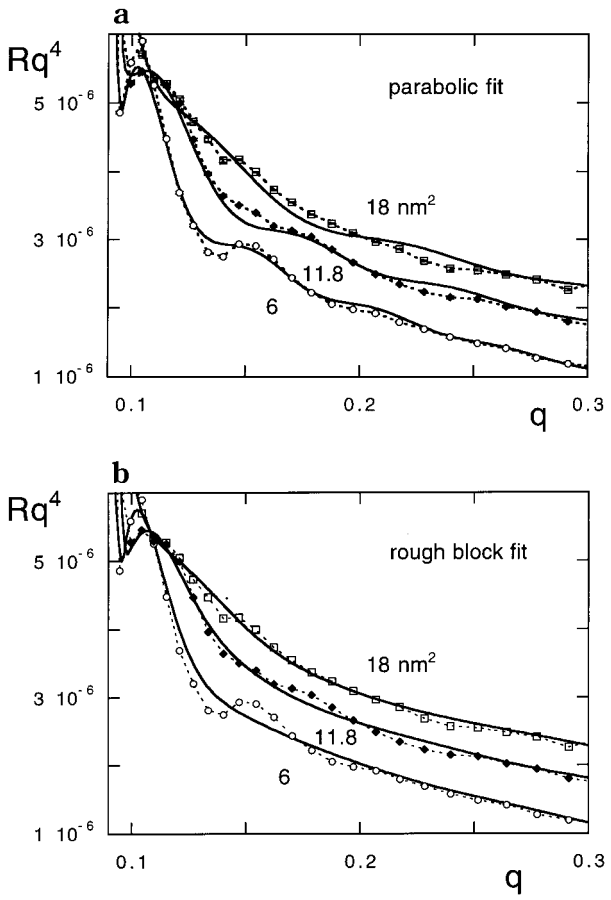

Figure 4. The measured reflectivities for three areas per molecule (symbols) and calculated reflectivities (solid curves) of (a) the best parabolic fit, and (b) the best block fit.

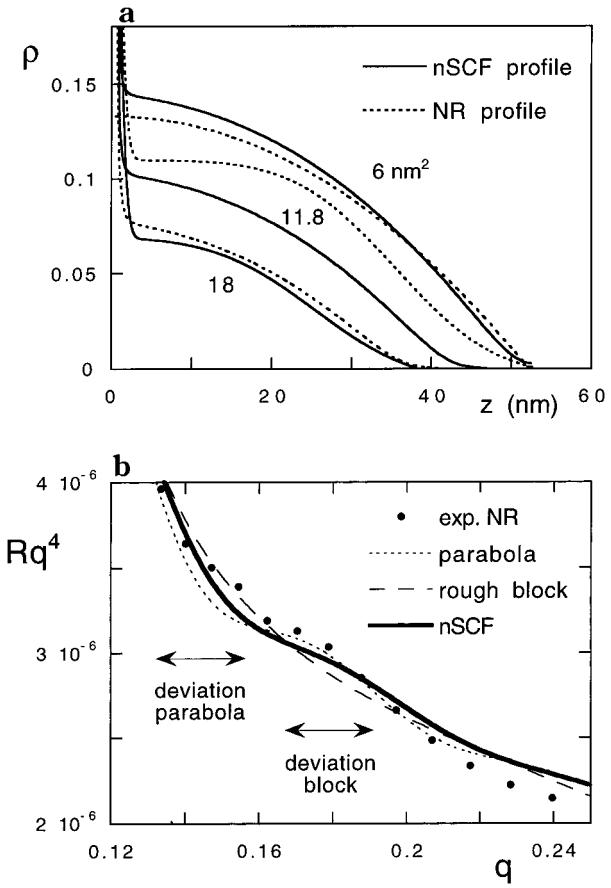

Figure 5. (a) The nSCF density profiles (solid curves) and the profiles of the best NR fits (dashed curves) for three areas per molecule. (b) Rq^4 versus q for two asymptotic models (rough block and parabola) and the nSCF profile.

characterize the difference between the coil and brush regime.) The solid curves denote the calculated reflectivities of the best parabolic fits, and the symbols are the measured reflectivities. In Figure 4b, the same is done for the fits of block profiles with roughness. In Figure 4a, it is clear that at low σ (18 nm^2), a parabolic reflectivity curve does not match the reflectivity well, whereas at the highest σ (6 nm^2), the match is quite good. In contrast, in Figure 4b, the match is rather good at low grafting densities and lessens as the grafting density increases.

From Table 1 and Figures 4a and 4b it can therefore be concluded that the best fit for the three lower σ is a block with a significant degree of roughness, whereas that of the highest σ is a parabolic fit. However, the difference in fit quality between a parabolic and block profile at the two intermediate values of σ is small, whereas the difference in fit quality between both profiles at the highest and lowest σ is significant. This result indicates that the density decay in the PEO brush at high σ is predominantly parabolic, whereas at low σ it is block-like close to the grafting surface and decays smoothly at the brush edge. At intermediate σ, the NR data suggest that the density profile contains characteristics of both profiles.

We can now compare the monomer density profiles obtained from the best fits of the NR spectra (either parabolic or a rough block) with the profiles predicted by our nSCF model. In Figure 5a the profiles are plotted for the same densities as those in Figure 4a,b. The dashed curves denote the profiles obtained from the best NR fits; the solid curves are the nSCF profiles for the same parameters as used in the surface pressure isotherms in Figure 2. The distal tail region, in which the density decreases exponentially towards zero, is

seen to be relatively extensive in the nSCF profile at the lowest σ, (i.e., 18 nm^2 per molecule). It can be expected that, provided that the PEO brush indeed has a tail region at this grafting density, it contributes significantly to the reflectivity spectrum. As the grafting density increases, the distal region diminishes in size in the nSCF profiles, and the profile 'steepens'. At the highest σ (6 nm^2 per molecule), the contribution of the distal tail region to the nSCF density profile is negligible, and the parabolic decay of the density is the prominent feature. Therefore, in this grafting regime, the parabolic decrease in density may be expected to be the dominant contribution to the reflectivity spectrum of the brush and the contribution of the tail region negligible.

This result corroborates the observed profiles of the best fits of the NR data (see Table 1). At low σ, a block profile with a significant roughness resembles the nSCF profile nicely. At the highest σ, the form of the parabolic profile agrees with the nSCF profile, although the predicted nSCF density is somewhat lower than that of the parabolic fit. At the intermediate value of σ, the quantitative agreement between the density profiles is less satisfactory. It can be observed that in this regime, the predicted nSCF profile contains features of both (asymptotic) models fitted to the NR data. It can thus be argued that, due to the combination of features of both models, the quantitative agreement is less than in the case where the nSCF profile corresponds closely to a fitted (asymptotic) model.

To verify this argument, we have calculated the reflectivity $R(q)q^4$ corresponding to the nSCF profile at a density 11.8 nm^2 per molecule (intermediate σ). To do this, we have used values for Γ_{D_2O} and ς_{int} equal to those obtained in experimental fits. Again we stress that, apart from insertion of the parameters just mentioned, no nSCF parameter has been fitted. In Figure 5b we have plotted $R(q)q^4$ versus q for the parabolic fit (short dashes), rough block fit (long dashes), and nSCF model (thick curve), together with the experimental data (dots). The length scale investigated in the q range in the figure, given by π/q, corresponds to the distance from the grafting plane at which the characteristic density gradient is found (10−30 nm). As seen in the figure, the reflectivity of the nSCF model follows the curve of the experimental data quite nicely. The optimized fits of a parabolic and block profile, however, show a q-range in which the deviation from the experimental data is significant. These ranges are indicated in the figure. Although the effects are subtle, Figure 5b indicates that in the intermediate σ regime, the nSCF profile, which combines features of the asymptotic block and parabolic model, is a better representation of the experimental density profile than either asymptotic model.

We can thus conclude that a true parabolic density profile, predicted by the aSCF model, is only obtained in brushes of $N \sim 10^3$ at relatively high σ. At low and intermediate values of σ, the profile is 'flattened' and the tail region, in which the density decays smoothly to zero, is relatively important. As mentioned in the *Introduction*, the distal tail region originates from fluctuations in the conformation of weakly stretched chain ends. Our results indicate that fluctuations of the chain ends of the grafted chains contribute strongly to the structure of the grafted layer up to high grafting densities. This outcome agrees with the nSCF calculations of Wijmans et al.[7]

Table 2. Area per Molecule According to Neutron Reflectivity Fits[a]

σ_{exp}^{-1}, nm^2	σ_p^{-1}, nm^2	σ_b^{-1}, nm^2
6.0	5.5	5.0
11.9	8.4	8.7
14.5	10.3	11.2
18.4	16.3	19.9

[a] Where σ_p^{-1} is the area of the parabolic model and σ_b^{-1} is that of the rough block model.

One could suggest that the fit parameter ς_b is a measure of the strength of the density fluctuations in the grafted layer. However, as shown in Table 1, ς_b is relatively constant as σ increases. A better measure, in our opinion, is the ratio ς_b/H. At low σ, the ratio ς_b/H is high and the structure of the grafted layer is strongly determined by the fluctuations. As ς_b/H decreases with increasing σ, the relative importance of the fluctuations decreases and the structure becomes increasingly parabolic. A true parabolic structure is found in the asymptotic limit $\varsigma_b/H = 0$.

We note that the other correction to the parabolic aSCF profiles, the depletion zone near the grafting plane, does not apply to our measurements. As we have mentioned, PEO strongly adsorbs to the air/water interface.[18,20] A depletion zone only occurs when the grafted polymer does not adsorb to the grafting plane and is not formed in our system.

It is interesting to determine whether the total monomer density, as found by fitting a block and parabolic model to the NR data, corresponds with that deposited experimentally. Such an integration is applied in some studies to determine σ, because this quantity is unknown during the measurement.[13] In our study, however, we know σ accurately. In Table 2 this amount is given for both fitted models, expressed as the area per molecule. It is clear that the agreement between the deposited amount and that according to the NR fit is reasonable for the parabolic model at the highest grafting density and for the rough block at the lowest. At intermediate densitites, however, the deposited and estimated amounts differ up to 30%. This result demonstrates that simultaneous determination of the brush structure and total deposited amount from NR data is sensitive to the applied model. Moreover, in the case that the fitted model is not suitable for the investigated density regime, the obtained values for σ via fitting of the NR data deviate significantly from the experimental values.

Finally, it can be checked whether the aSCF scaling law for the brush height as a function of the grafting density, $H \sim \sigma^{1/3}$, holds in these NR measurements. In our previous paper, the aSCF scaling law was concluded to be correct for long PEO brushes.[20] If H, obtained by fitting a parabolic profile, is plotted as a function of σ an exponent of 0.36 is found. Interestingly, fitting the results of the rough block yields the same power exponent. The height of the layer in the rough block model and that in the parabolic model vary by a constant for the four measured densities; namely, 1.3. Although the number of data points is limited, this result corroborates our previous conclusion that the aSCF scaling law of H as a function of σ is valid in this regime.[20]

4. Bimodal Brushes

We continue with the analysis of the NR data for bimodal PEO brushes. Three samples were measured

Table 3. The Examined Bimodal Brush Layers

sample	N_1,N_s	mixing ratio l:s	no. measured densities
Bbl	700, 148	1:5	4
Bb2	700, 250	1:5	5
Bb3	700, 148	1:3	3

Table 4. Results for Biparabola Fits for Bb1, Bb2, and Bb3 Series

area, nm^2	π	ρ_1	H_1	ρ_2	H_2	χ^2
15, 75	11.0	0.063(2)	7(1)	0.0198(3)	27.8(6)	0.85
10, 50	11.9	0.099(3)	7.1(9)	0.0470(3)	28.3(8)	1.66
7, 35	16.0	0.105(2)	8.5(6)	0.0472(4)	32.4(6)	1.26
5, 25	22.3	0.104(3)	12.0(4)	0.0602(3)	34.3(8)	0.75
15, 75	12.1	0.0275(2)	11(1)	0.0468(3)	27.8(8)	0.59
12, 60	13.0	0.0475(3)	10.2(9)	0.0535(4)	26.9(6)	0.54
10, 50	14.2	0.048(3)	14(1)	0.0643(3)	30.0(8)	0.42
8, 40	16.4	0.0544(2)	14.8(8)	0.0696(4)	31.9(6)	0.78
6.5, 32.5	21.0	0.0694(3)	19.7(6)	0.080(3)	37.4(8)	0.75
10, 30	12.1	0.274(4)	1(1)	0.0636(2)	29.0(6)	1.21
7, 21	14.7	0.0184(4)	8(1)	0.0743(3)	31.3(5)	0.95
5, 15	22.3	0.0629(3)	11.1(4)	0.100(2)	41.3(8)	0.69

at various grafting densities. The chain lengths, mixing ratios, and number of measurements are listed in Table 3. As shown, the ratio of chain lengths N_l and N_s in the series Bb1 and Bb3 is ~5, and that in Bb2 ~3. According to the predictions of the aSCF and nSCF models, such ratios should result in bimodal brush structures.[22,23]

The NR data were fitted to models consisting of a single block or two blocks with and without roughness, a single parabola and two parabolas, and a combination of a parabola and a block. The total monomer density at a given distance z is simply the sum of the densities of both blocks in the diblock or double parabola model at that distance (or the density of the longer block if $z > H_1$, where H_1 is the height of the brush formed by the shorter chains; see Figure 1). In general, a single block or two blocks without roughness did not give a good fit of the NR data, similar to the NR fits of the monodisperse brush. Moreover, the single block and single parabola gave fits of significant less quality than the two blocks or parabolas.

In the Bb1 series, the fit quality of a model of two parabolas and two rough blocks was, roughly speaking, equivalent. The values for the biparabola fit parameters are listed in Table 4. In Figure 6a, Rq^4 is plotted versus q for a part of the q range. The points denote the experimental reflectivities, and the solid curves are the best fit of a biparabola model. The dashed curves through the experimental points are a guide for the eye. It can be seen that the the fitted reflectivities agree quite nicely with the measured ones, although at some values of q, the measured reflectivities clearly differ from the fitted. The same result is found when the reflectivities of a model of two blocks are compared with the experimental. This entails that representation of the grafted layer as either a biparabolic structure or the sum of two blocks with an exponentially decaying tail is reasonable, but does not fully represent the density profiles in the grafted layer.

As suggested by a referee, however, the large difference in relative grafting density between the short and long chains could result in a parabolic structure close to the interface and a more block-like structure in the distal region. This type of structure should corroborate the density profile for the monodisperse brush at low σ, discussed in the previous section. To check this, we also fitted the NR data to a model consisting of a

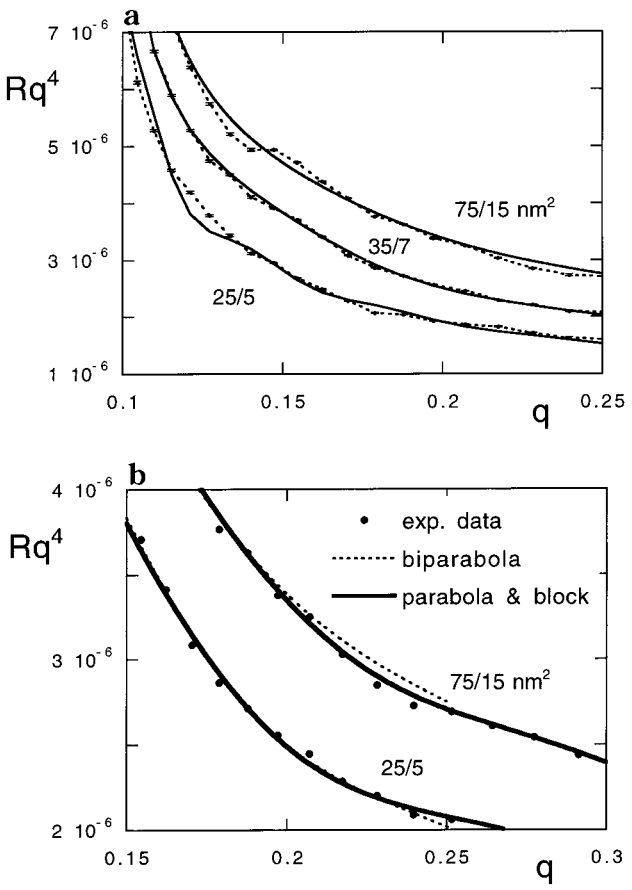

Figure 6. (a) Rq^4 versus q for the Bb1 series at three grafting densities. The points denote the experimenal reflectivities, and the solid curves denote the reflectivities of the best fits of a biparabolic model. (b) Rq^4 versus q for a model consisting of a combination of a parabola and a block and a biparabolic model for two grafting densities.

combination of a parabola and a rough block. For the two lowest grafting densities in the Bb1 series, this combination gave a slightly better result than a double parabola, and for the two high values of σ, the result was approximately equivalent. The subtle difference in the reflectivity spectra of both models is shown in Figure 6b for low σ and high σ. At low σ, the biparabolic model has a small but significant deviation from the experimental data at intermediate values of q. This deviation is located at higher values of q than the deviation found for a single parabolic model in Figure 5b because the grafting density of the long chains in the Bb1 series at low σ is lower than that in the monodisperse brush (75 nm^2 and $\pm$15 nm^2, respectively).

The nSCF density profile for the two lower grafting densities of Bb1 is compared with the profile resulting from fitting a parabola-block model in Figure 7a, and the nSCF profiles are compared with those of the biparabolic model in Figure 7b. As mentioned in *Section 2*, no free parameters were used to obtain these nSCF curves. In the nSCF profiles, the monomer density decreases strongly in the inner layer of the bimodal brush, whereas the decay is more gradual in the periphery. This feature is also found in the NR profiles. A remarkable feature of both figures is the fact that the height of the inner and outer layers, found by fitting the NR data to a biparabolic model, is in good agreement with the nSCF profiles. Although the bimodal structure in the nSCF profiles is considerably less pronounced at low values of σ than at high, the fitted height of the

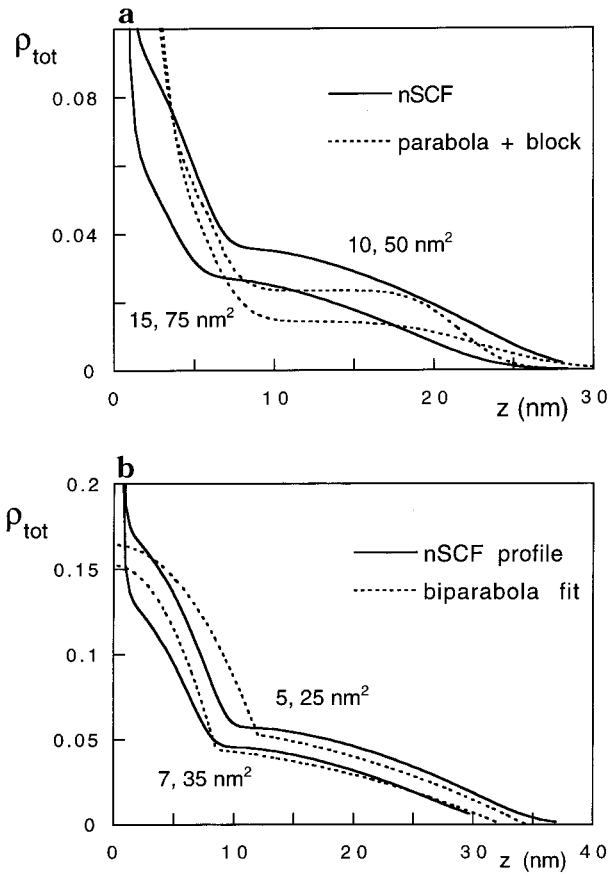

Figure 7. The nSCF density profiles (solid curves) and profiles of the best NR fits (dashed curves) for $N(150):N(700)$ of 5:1 for (a) the two low grafting densities and (b) two high grafting densities.

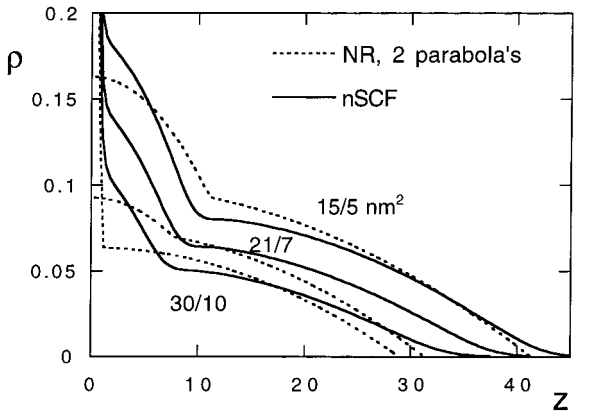

Figure 8. Same as Figure 7 (a and b) for $N(250):N(700)$ of 5:1 and three grafting densities.

inner layer agrees well with the expected height. The boundary of the inner layer (i.e., H_1) corresponds to a sharp change in the density gradient. It appears that the NR fits are sensitive to the position of this boundary. The quantitative agreement of the density profiles is good at high grafting densities, but less satisfactory at lower densities. The reason for this difference may be the low overall monomer densities in this regime and subsequent small difference in scattering length densities of the polymer layer and subphase.

In Figure 8 the profiles resulting from the best NR fits and the nSCF density profiles are plotted for three grafting densities of the Bb2 series. The best fit at low σ is that of a parabola-block model and at other densities

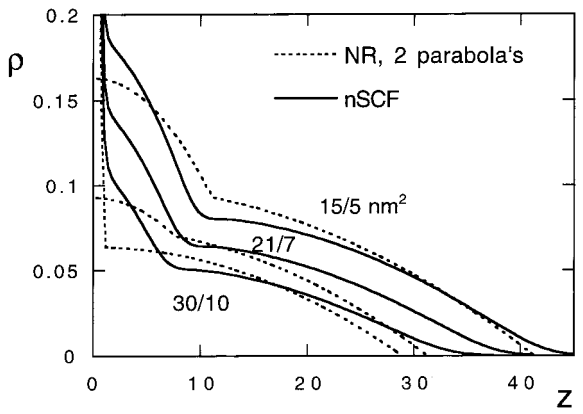

Figure 9. Same as Figure 7 (a and b) for $N(150):N(700)$ of 3:1 and three grafting densities.

a biparabola model. As shown in Table 2, the mixing ratio of this series is the same as that of the Bb1 (i.e., 1:5), but the short block consists of 250 instead of 148 monomers. It is thus expected that H_1 and H_2 differ less than in the Bb1 series. This expectation is confirmed by the fits of the NR data. As is the case for the Bb1 series, the agreement of H_1 and H_2 of the NR fits and the nSCF profiles is good, whereas the agreement in monomer density is less quantitative.

In Figure 9 the same kind of plot is shown for the Bb3 series. The length ratio is the same as in the Bb1 series, but the mixing ratio is 1:3, whereas it is 1:5 in the Bb1 series. As a result, the contribution of the smaller chains in the Bb3 series to the density profile is significantly less than that in the Bb1 series. This difference is clear from the nSCF profiles in Figure 9. At the lowest σ, the contribution of the short chains to the nSCF density profile is minor. This minor contribution is reflected in the fitted value of H_1 in Table 4. No reasonable value for H_1 is found using a model consisting of two parabolas, two blocks, or a combination. With increasing σ, the contribution of the short chains increases and the quality of the biparabolic fit subsequently increases. Thus, the layer structure, determined experimentally from NR, is consistent with a bimodal structure in the case that the nSCF density profile can be clearly separated into a proximal and distal regime. At the lowest σ, the fit of a model consisting of a single and double parabola is roughly equivalent. In this case, the (subtle) bimodal structure, as observed in the nSCF profile, is not discerned from the NR data.

It is interesting to examine to what extent the long block is additionally stretched due to the presence of the shorter chains. In other words, how far out is the longer chain pushed by the underlying layer? In Figure 10 the total height of the bimodal brushes (i.e., H_2) is plotted as a function of the area per long chain. The curve is the power law fit of the height of the monodisperse brush as a function of the area per chain, fitted by a parabolic model. It is clear that the total brush height in the Bb1 and Bb2 series is significantly above that of the monodisperse brush, whereas that of the Bb3 series is comparable to it. Moreover, the additional extension of the Bb1 series is less than that of the Bb2 series.

The data in Figure 10 can be understood by considering the mixing and chain length ratios. The mixing ratio of the Bb1 and Bb2 series is equal, but the lengths of the short block are 148 and 250, respectively. This difference in length causes, at a given grafting density,

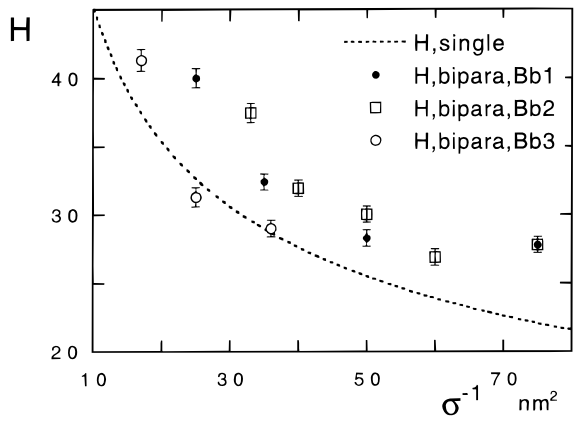

Figure 10. The additional stretching of the long PEO chains ($N = 700$) in bimodal brushes as a function of the area per molecule of the long chains. The dotted curve is the fit through the height in a parabolic model of the monodisperse brushes for $N = 700$. The symbols denote the total brush height in the bimodal brushes at the same area per long chain.

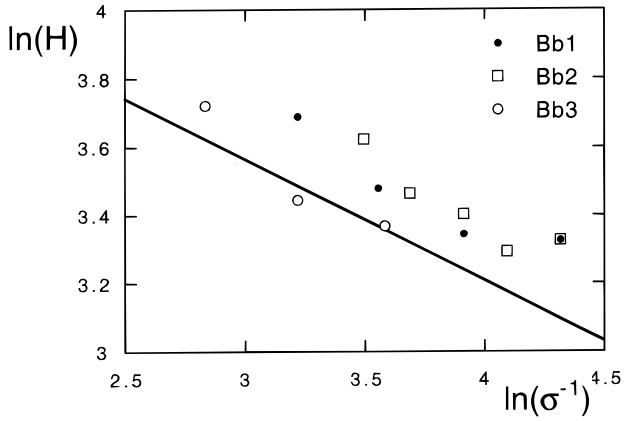

Figure 11. The results of Figure 10 plotted double-logarithmically. The solid line is the fit of results for the monodisperse PEO brush, with an exponent of 0.36. The symbols are the bimodal results.

the thickness of the inner layer in the Bb2 series to be larger than that in Bb1 and the outer layer to be pushed further from the grafting plane. The length ratios of the Bb1 and Bb3 series are equal, but the mixing ratio is 1:5 and 1:3, respectively. At a given area per long block, the number of grafted short chains is significantly less in the Bb3 series and, therefore, the additional stretching of the long chains is small. Apparently, the number of short chains in the Bb3 series is not high enough to cause a significant increase in extension with respect to the monodisperse brush. Therefore, as expected, the height of the bimodal brush at a given grafting density of long chains increases with increasing length and increasing grafting density of the shorter chains.

Finally, as predicted by aSCF models for bimodal brushes, the same power law should hold for the overall height as a function of σ in a bimodal brush, at fixed length and mixing ratio, as the one applicable to a monodisperse brush, i.e., $H \sim \sigma^{1/3}$.[21,22] In Figure 11 the overall brush height is plotted as a function of the area per molecule of the long block in a double logarithmic plot. The solid curve is the best fit of the data of the monodisperse PEO brush, and the symbols are the results for bimodal brushes. It is clear that the results of the Bb1 and Bb2 series follow the aSCF power law, with the exception of the lowest grafting density. This 'exception', however, is not surprising: at this σ, the surface pressure is not far above the saturated surface pressure and the PEO chains are only partially 'pushed' into the water phase. Thus, the condition of strong stretching of the chains is not met, and the aSCF power law is not obeyed.

5. Discussion and Conclusions

The structure of polymers end-grafted at high densities (brushes) has been investigated theoretically in numerous studies with various models. Experimental verification of these models, however, is not a moot issue. In this paper we investigated PEO brushes at the air/water interface with NR. Analysis of the NR data with various models and comparison of the density profiles of such models with theoretical predictions yields insight into the structure of such grafted layers and how such structures may be controlled.

Monodisperse PEO brushes, consisting of chains of uniform length, were investigated at several (high) grafting densities. Previous analysis of the surface pressure isotherms demonstrated that at these grafting densities, the grafted layer is expected to assume a brush conformation.[20] Analysis of the NR data shows that at relatively low grafting densities, the monomer density profile of the brush is rather flat and has an extended tail region, in which the monomer density drops smoothly to zero. As the grafting density increases, the gradient in monomer density increases, and at high grafting density the profile is predominantly parabolic. This parabolic profile has been predicted by aSCF models for brushes. The increase of the brush height with increasing grafting density obeys the aSCF scaling law (i.e., $H \sim \sigma^{1/3}$).

Our results for monodisperse brushes corroborate and improve on the results for PEO brushes of Bijsterbosch et al.[18] They contradict, however, those of Richards et al., who concluded that NR is not suitable for investigating the structure of a hydrogenated polymer layer on D_2O.[17] In this paper we demonstrated that not only can the height of a hydrogenated PEO brush on D_2O be examined, but also the internal structure of the brush. The reason for the failure of Richards et al. to find a brush-like structure of poly(methylmethylacrylate) poly(ethylene oxide) spread at the air/water interface is simple: their NR measurements were done at surface pressures up to 6 mN m^{-1}, whereas our measurements were done at significantly higher surface pressures (see Figure 2). Thus, in the study of Richards et al., the grafting densities are low, so that adsorption of PEO chains to the air/water interface results in flat structures, also known as 'pancakes'.[18] As shown in this paper, a true parabolic density profile in the brush is only obtained at very high grafting densities, of the order 10 mg m^{-2}. The grafting densities measured by Richards et al. were 0.6 and 1.2 mg m^{-2}.[18] Clearly, a brush structure cannot be expected at such low densities.

Bimodal brushes were made by mixing two PEO block lengths at a given mixing ratio. Analysis of NR data of such bimodal brushes clearly revealed the bimodal structure of the PEO layer. The small chains are found close to the surface, whereas the long chains protrude through this proximal layer into the bulk phase. It is shown that at a given area per long PEO chain, the long chains in a bimodal brush are more strongly stretched than those in a monodisperse brush because of the

presence of the grafted short chains. This additional stretching increases with increasing number of short chains per long chain and increasing length of the short chains.

The experimental monomer density profiles, obtained by fitting the NR data to several models, are compared with the density profiles predicted by the Scheutiens−Fleer nSCF model. Good agreement between the surface pressure isotherms of monodisperse brushes in the nSCF model and the experimental isotherms demonstrates that thermodynamic variables, such as the surface pressure, are correctly modeled in the nSCF model. Good agreement between the nSCF model and the experimental results is also found for structural properties (i.e., the monomer density profiles). The density profile of a monodisperse brush at low grafting density obtained from analysis of the NR data is a relatively flat profile with an extended tail region. This experimental density profile corresponds quantitively with the numerical profile. At high grafting density, the best fit of the NR data is a parabolic profile, which also agrees well with the numerical profile. At intermediate grafting densities, the numerical profiles display both a parabolic decay in monomer density and an extended tail region. This profile is corroborated by the equal fit quality of a parabolic model and a block with extended tail region from the NR data.

In the case of bimodal brushes, the agreement between the NR data and nSCF profiles for the thickness of the inner and outer layer is quite good. The quantitative agreement of the density profiles, however, is less than that of monodisperse brushes. It is shown that in the case that two regions can not be clearly discerned in the nSCF density profile, a bimodal density profile does not fit the NR data well.

A small comment can be made with respect to lateral inhomogeneities in the bimodal brush layer. One may ask whether the long and short PEO chains can phase separate into regions relatively rich in short chains and regions relatively rich in long chains. Such phase separation was never observed in the surface pressure isotherms or with Brewster angle microscopy. It can be argued, however, that such phase separation does not occur in the PEO bimodal brushes in general. Phase separation generally originates from unfavorable energetic interactions, and is tempered by the mixing entropy. In the case of chemically different grafted chains (i.e., PS−PEO and PS−PVP), such unfavorable energetic interactions may be expected to occur. However, because in our study the short and long chains are chemically equivalent, such interactions are not present, and the mixing entropy ensures a homogeneous monolayer.

We conclude that the combination of NR with nSCF models is an excellent manner for investigating the internal structure of grafted polymeric layers in contact with a solvent in detail. Experimental verification of the predicted layer structure via NR demonstrates the predictive power of nSCF models, whereas comparison of the numerical results with results obtained from fitting various models to the NR data demonstrates the detail in structure that can be discerned with NR.

Acknowledgment. This study was supported by the Training and Mobility of Researchers Programme for Large-scale Facilities of the European Union. We thank J. Webster for his help with the preparation of the NR data. We also thank the referee for his valuble suggestions.

References and Notes

(1) Alexander, S. *J. de Phys. Fr.* **1977**, *38*, 983.
(2) de Gennes, P-G *Macromolecules* **1980**, *13*, 1069.
(3) Milner, S. T.; Witten, T. A.; Cates, M. E. *Macromolecules* **1988**, *21*, 2610.
(4) Zhulina, E. B.; Borisov, O. V.; Priamitsyn, V. A. *J. Colloid Interface Sci.* **1990**, *137*, 495.
(5) Whitmore, M. D.; Noolandi, J. *Macromolecules* **1990**, *23*, 3321.
(6) Murat, M.; Grest, G. S. *Macromolecules* **1989**, *22*, 4054.
(7) Wijmans, C. M.; Scheutjens, J. M. H. M.; Zhulina, E. B. *Macromolecules* **1992**, *25*, 2657.
(8) Witten, T. A.; Leibler, L.; Pincus, P. A. *Macromolecules* **1990**, *23*, 824.
(9) Milner, S. T. *J. Chem. Soc. Faraday Trans.* **1990**, *86*, 1349.
(10) Auroy, P.; Auvray, L.; Leger, L. *Phys. Rev. Lett.* **1991**, *66*, 719.
(11) Auroy, P. A.; Leger, L. *Macromolecules* **1991**, *24*, 2523.
(12) Field, J. B.; Toprakcioglu, C.; Ball, R. C.; Stanley, H. B.; Dai, L.; Barford, W.; Penfold, J.; Smith, G.; Hamilton, W. *Macromolecules* **1992**, *25*, 434.
(13) Kent, M. S.; Lee, L. T.; Farnoux, B.; Rondelez, F. *Macromolecules* **1992**, *25*, 6240.
(14) Factor, B. J.; Lee, L. T.; Kent, M. S.; Rondelez, F. *Phys. Rev. E* **1993**, *48*, 2354.
(15) Karim, A.; Satija, S. K.; Douglas, J. F.; Ankner, J. F.; Fetters, L. J. *Phys. Rev. Lett.* **1994**, *73*, 3407.
(16) Richards, R. W.; Rochford, B. R.; Taylor, M. R. *Macromolecules* **1996**, *29*, 1980.
(17) Richards, R. W.; Rochford, B. R.; Webster, J. R. P. *Polymer* **1997**, *38*, 1169.
(18) Bijsterbosch, H. D.; de Haan, V. O.; de Graaf, A. W.; Mellema, M.; Leermakers, F. A. M.; Cohen Stuart, M. A.; van Well, A. A. *Langmuir* **1995**, *11*, 4467.
(19) Lekner, J. *Theory of Reflection*; Martinus Nijhof: Dordrecht, 1987.
(20) Currie, E. P. K.; Leermakers, F. A. M.; Cohen Stuart, M. A.; Fleer, G. J. *Macromolecules* **1999**, *32*, 487.
(21) Milner, S. T.; Witten, T. A.; Cates, M. *Macromolecules* **1989**, *22*, 853.
(22) Birshtein, T. M.; Lyatskya, Y. V.; Zhulina, E. B. *Polymer* **1990**, *31*, 2185.
(23) Dan, N.; Tirrell, M. *Macromolecules* **1993**, *26*, 6467.
(24) Kent, M. S.; Factor, B. J.; Satija, S.; Gallagher, P.; Smith, G. S. *Macromolecules* **1996**, *29*, 2843.
(25) Haruska, Z.; Hurtrez, G.; Walter, S.; Riess, G. *Polymer* **1992**, *33*, 2447.
(26) *Handbook of Mathematical Functions*; Abramowitz, M.; Stegun, I. A., Eds.; Dover: New York, 1972.
(27) Penfold, J.; Richardson, R. M.; Zarbakhsh, A.; Webster, J. R. P.; Bucknall, D. G.; Rennie, A. R.; Jones, R. A. L.; Cosgrove, T.; Thomas, R. K.; Higgins, J. S.; Fletcher, P. D. I.; Dickinson, E.; Roser, S. J.; McLure, I. A.; Hillman, A. R.; Richards, R. W.; Staples, E. J.; Burgess, A. N.; Simister, E. A.; White, J. W *J. Chem. Soc., Faraday Trans.* **1997**, *93*, 3899.
(28) Cao, B. H.; Kim, M. W. *Faraday Discuss.* **1994**, *98*, 245.
(29) Brandrup, J.; Immergut, E. H. *Polymer Handbook*, 3rd ed.; Wiley: New York, 1989.
(30) Faraone, A.; Magazu, S.; Maisano, G.; Migliardo, P.; Tettamanti, E.; Villari, V. *J. Chem. Phys.* **1999**, *110*, 1801.
(31) Finch, C. A. *Chemistry and Technology of Water-soluble Polymers*, Plenum: New York, 1983.

MA990936W